Sensor and Simulation Notes

Note 365

2 February 1994

Reflector IRA Design and Boresight Temporal Waveforms

D. V. Giri

Pro-Tech, 3708 Mt. Diablo Boulevard, #215

Lafayette, CA 94549-3610

and

Carl E. Baum

Phillips Laboratory

Abstract

The IRA considered here is a paraboloidal reflector fed by conical TEM lines. Such an IRA has been analyzed in the past for its performance characteristics such as the prepulse or feed step and the impulse, assuming a step function excitation. In this note, we extend the analysis to include the diffracted fields from the launcher plates and the circular rim of the reflector. The diffraction from the launcher plates can be viewed to consist of two parts. One has the plate edge diffraction followed by diffraction associated with the total currents on the plates. The leading terms in all of these diffracted signals arriving at an observer in the far field have been determined in this note.

I. Introduction

The radiated field from an aperture antenna consists of a spatial integration of the aperture fields over the aperture, while the temporal behavior of the aperture field get differentiated. This is a simple physical fact well exploited in an IRA, proposed by Baum [1]. One form of an IRA then consists of a paraboloidal reflector fed by conical transmission lines that propagate a spherical TEM wave emanating from the focal point of the reflector. There are several factors that govern the design of an optimal IRA [1 to 5], some of which are listed below:

i) The aperture area should be as large as practical, since the far field is proportional to the square root of this area for a constant voltage at the feed. (The far field is proportional to the aperture area for a constant aperture field.)

ii) The feed plates should be narrow to reduce aperture blockage, resulting in high values (several 100's of Ω) of feed-impedance.

iii) It is preferable to have 2 pairs of feed plates for symmetric illumination of the radiating aperture. Since the two pairs are connected in parallel, this also halves the load impedance for the pulse generator at the focal point.

iv) The feed plates, which are triangular in shape can in principle, face each other or be coplanar (Figure 1). Coplanar feed plates are preferred since their aperture blockage effect is smaller.

v) The terminating impedances at the junctions of feed plates and the reflector rim can be tuned to balance the late-time electric and magnetic dipole moments of such an IRA.

vi) The pulse generator should be of the differential type in the case of a full IRA. It can be single-ended if half an IRA is built using an image plane. A single-ended pulse generator driving a full IRA could result in both differential and common mode currents on the feed plates, unless a fast, high-voltage balun is used. Alternatively, one can use the antenna conductors as part of the balun [2]. While the differential mode currents are desirable, the common mode currents can distort the desired features

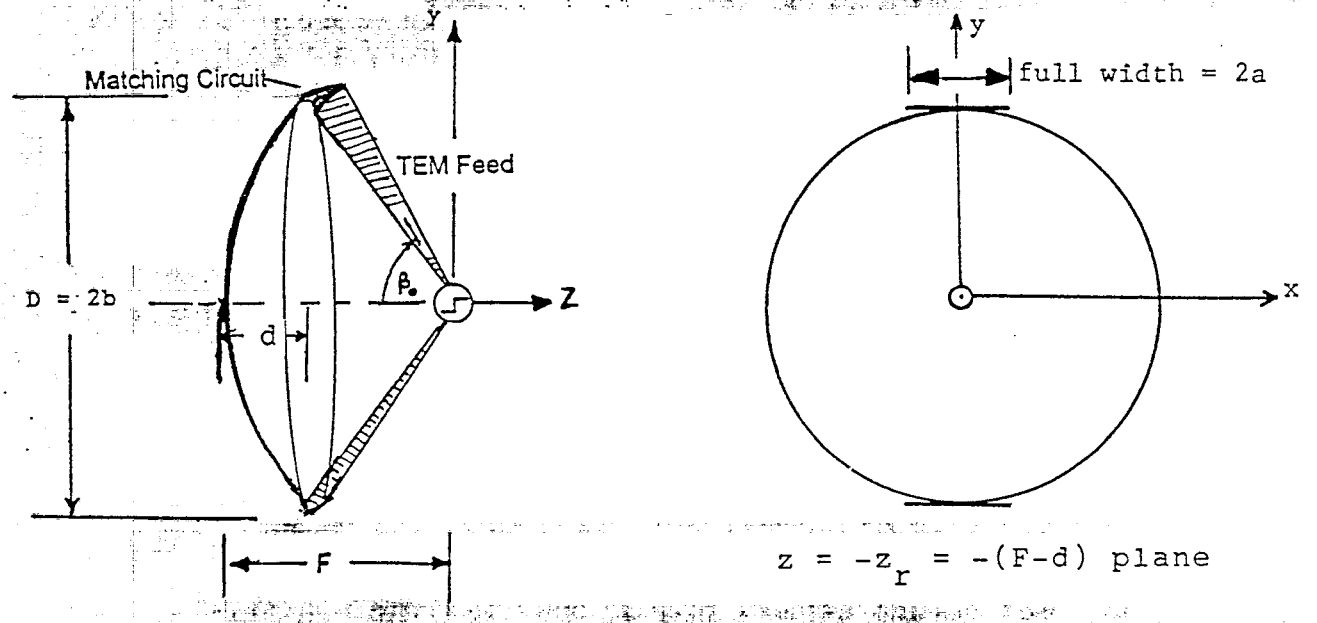

(a) Facing plates

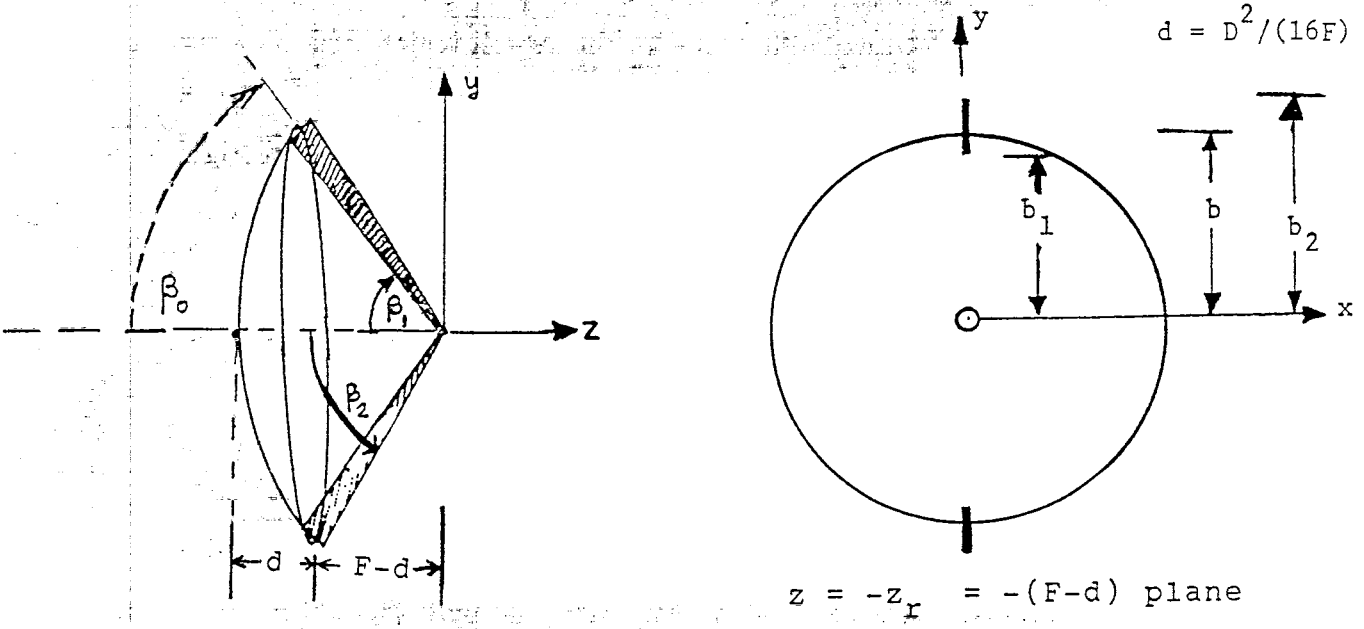

(b) Coplanar plates in $x = 0$ plane

Figure 1. Two possible ways of TEM feed

in the far field. Care must be taken to avoid undesirable currents flowing on the outer shield of the feed cable(s).

vii) The pulse generator can be represented by a single switch near the focal point. The two electrodes of the switch shall be at equal but opposite potentials $\pm V(t) = \pm(V_0/2)\, f(t)$.

viii) Since the far field on axis is proportional to the rate of rise of the applied voltage $(\partial V/\partial t)$, one would like to maximize this rate of rise. This leads to physically small switches operating in a high-pressure gas tending to approach 10^{15} V/s (e.g., 100 kV in 100 ps).

ix) The combination of requiring physically small switches, high voltages and fast rise times implies the use of electromagnetic lenses in the switch region. The lens can be made of an oil medium which serves the dual purposes of high-voltage insulation and ensuring a spherical TEM wave launch on to the feed plates.

A careful consideration of the above listed factors leads one to an optimal IRA comprising of a paraboloidal reflector fed by two pairs of coplanar feed plates as indicated in Figure 2. An expanded view of the switch region including the lens is shown in Figure 3. What the lens does, is to ensure that the wavefront of the TEM wave in the air region outside the lens medium is spherical with its origin at the focal point of the parabolic reflector which is also the true apex of the feed plates.

We also assume that the switch located at $z = -z_s$ in Figure 3 closes at a time $t = t_1 = [\{\ell_1(1 - \sqrt{\mathcal{E}_r}) + z_s\sqrt{\mathcal{E}_r}\}/c]$ so that in effect, an ideal source turns on at $t = 0$ at the apex and the wave propagates in air. In the expression for t_1, ℓ_1 is the length of the lens along the negative z axis as indicated in Figure 3. The lens medium (e.g., oil in a container whose dielectric constant is the same as oil) also helps in high-voltage stand off. It is further noted that the lens lowers the characteristic impedance of conical transmission line by $(1/\sqrt{\mathcal{E}_r})$ except for small changes due to angles. $\mathcal{E}_r$ is the dielectric constant of the lens medium (e.g., oil with $\mathcal{E}_r \simeq 2.25$). This change in dielectric constant, also increases early-time field due to transmission coefficient of the electric field (TEM voltage) (> 1) in going

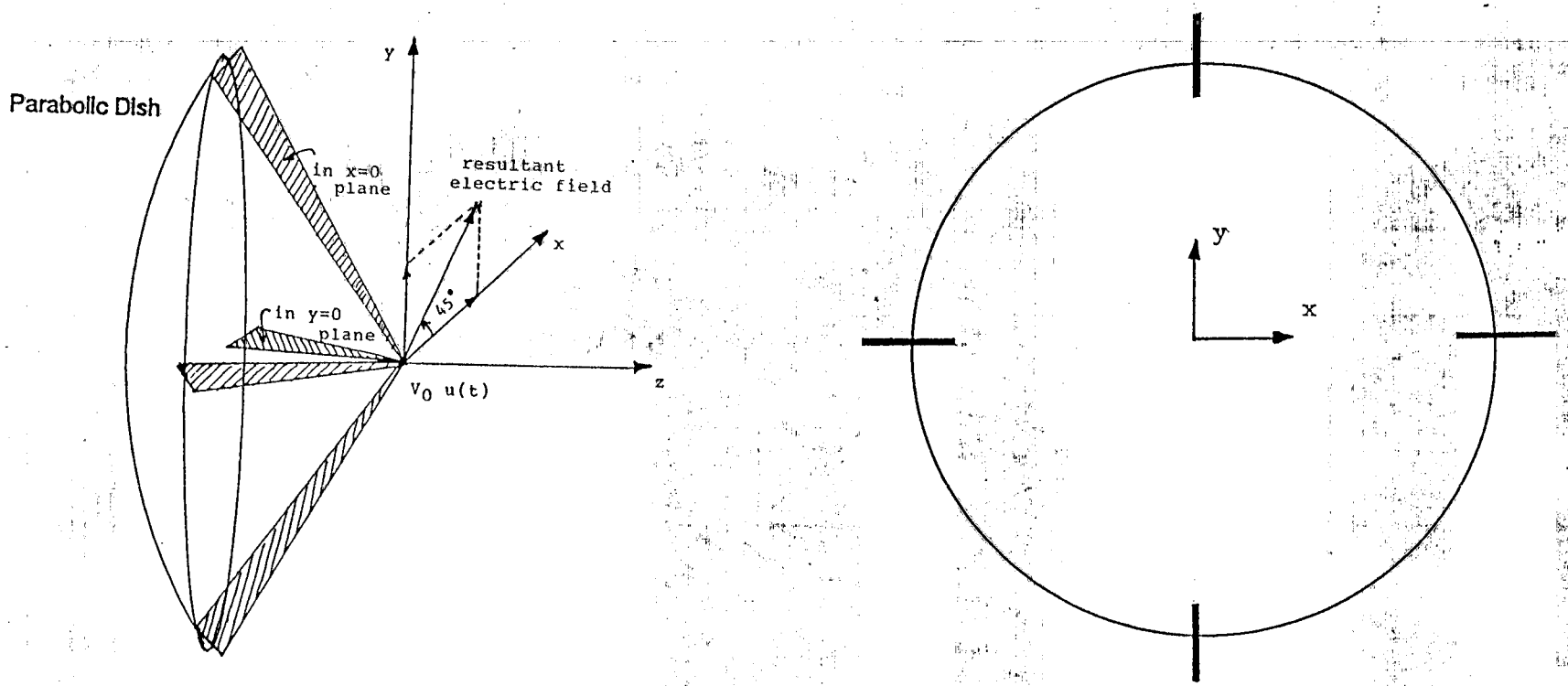

Figure 2. An example IRA fed by a pair of coplanar conical TEM lines.

NOTES

a) Adjacent plates are tied together near the apex which halves the net impedance.

b) The load on the pulser is half of $Z_c^{(\mathrm{TEM})}$ of either pair.

c) The resultant boresight radiation is along a 45° angle $\phi = 45°$ in the x-y plane.

d) One can rotate the above structure by 45° so that the resultant E-field is oriented along $\vec{1}_y$ direction in the far field.

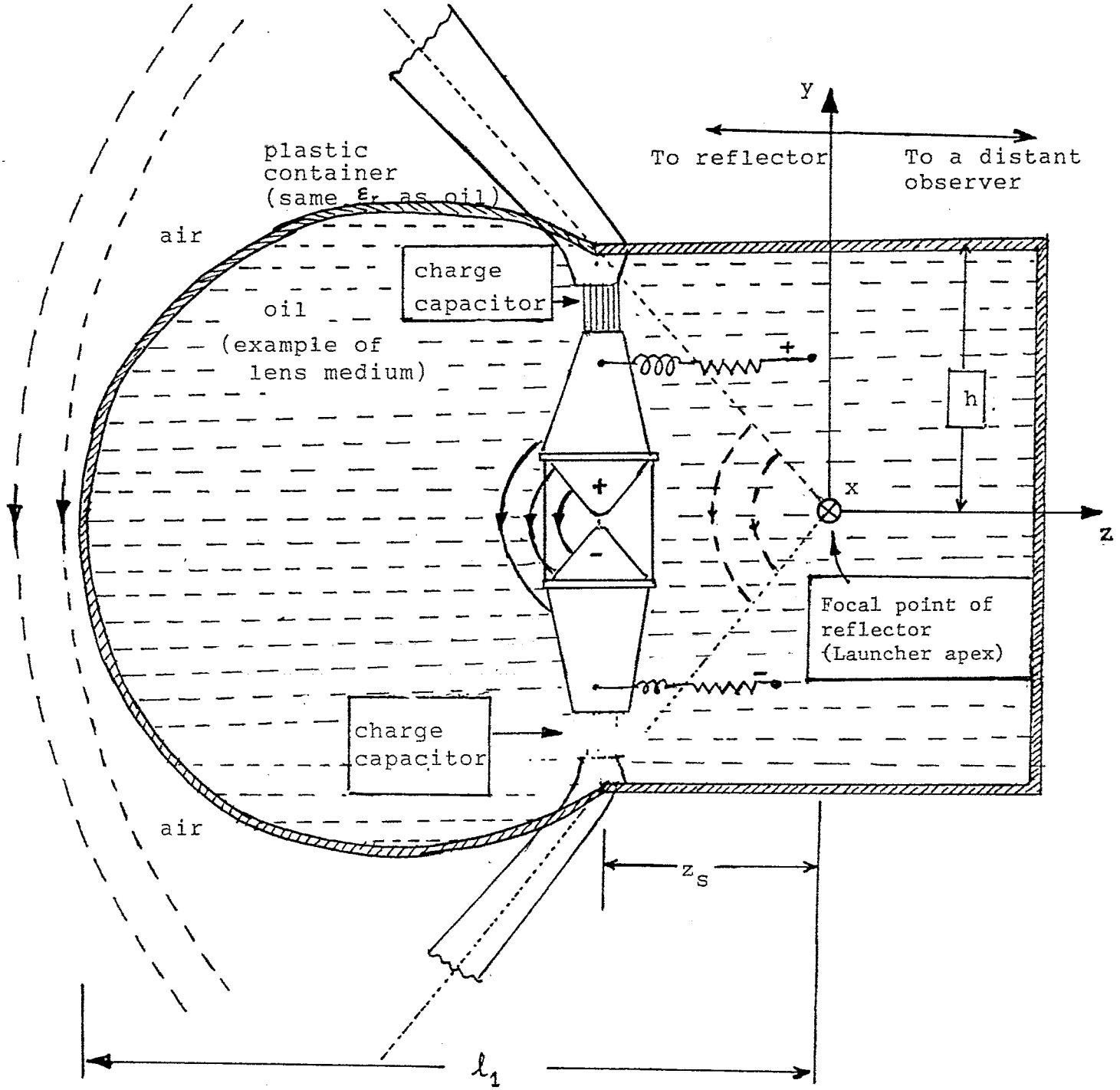

Figure 3. An expanded view of the launch region of the IRA in Figure 1 (switch center is located at $z = -z_s$).

from the lens dielectric to air.

Next, we turn our attention to the radiated waveform on boresight of an optimally designed IRA. Although our interest is in the performance characteristics of an IRA fed by 4 plates as in Figure 2, it is adequate to consider the canonical problem of an IRA fed by 2 plates as in Figure 1b. The resultant radiated field for the 4 plates can be obtained by a superposition of the fields for each set of two plates. As shown in Figure 2, the resultant field for 4 plates is along a $\phi = 45°$ direction. We then note that the formulae developed in this note are for the case of 2 plates with an applied potential of $V_0\, u(t)$ between the two plates. To obtain the corresponding results for the 4 plate situation, we observe that the geometric factor f_g should be multiplied by $(1/2)$ to account for the parallel connection of the two sets of plates. Likewise, the radiated fields amplitudes should be multiplied by $\sqrt{2}$, while noting a new principal direction at 45°. These changes are required in going from 2-plate feed to 4-plate feed via vectorial additon of x and y components of the radiated field.

We also emphasize that we have considered an ideal excitation of $V_0\, u(t)$. In practice the applied voltage will have a finite rise time, e.g., $V_0(1 - e^{-at})\, u(t)$ and the radiated fields in this note will have to be suitably modified for the finite-rise excitation via convolution integrals.

Having outlined the IRA, its feed configuration and launcher considerations, we proceed in Section II with a characterization of its performance in terms of the time-domain far field on boresight.

II. Boresight Radiation

The basic principles of an IRA illustrated in Figures 1 and 2 are by now, well analyzed and understood [1, 5 and 6]. When this form of IRA was originally proposed [1], the boresight radiation was predicted to consist of a feed-step followed by an impulse-like behavior as indicated in Figure 4 for a step function source. Later numerical analysis [4] produced a similar radiated wave as shown in Figure 5. Of late, the emphasis has shifted to obtaining closed-form expressions for various temporal elements of the boresight radiation [5 and 6]. We can build on the past analyses, and conceptually list the various temporal elements of the boresight radiation as follows, assuming that the step-function pulse generator is switched on at $t = 0$, and the observer is at a distance r $(= z)$ to the right of the focal point of the parabola. The focal point coincides with the theoretical apex of the launcher plates. These elements are:

A. *Prepulse*—

1) feed step

B. *Main pulse of interest*

2) impulse

C. *Postpulse*

3) feed plate diffraction consisting of two parts

a) plate edge on plate of finite width, large compared to wavelength

b) plate of finite width, small compared to wavelength, modelled by circular cylinder

4) edge diffraction from the circular rim of the parabolic reflector

D. *Constraints on entire pulse*

5) low-frequency dipole moment radiation and no radiation at zero frequency (dc).

We now discuss each of the above elements.

1) *Feed step or pre-pulse* $[t_r \leq t \leq (t_r + 2F/c)]$

This is a direct radiation from the source or the "switch" towards the observer. It starts at a time $t = t_r = (r/c)$ and lasts for a duration approximately $= (2F/c)$.

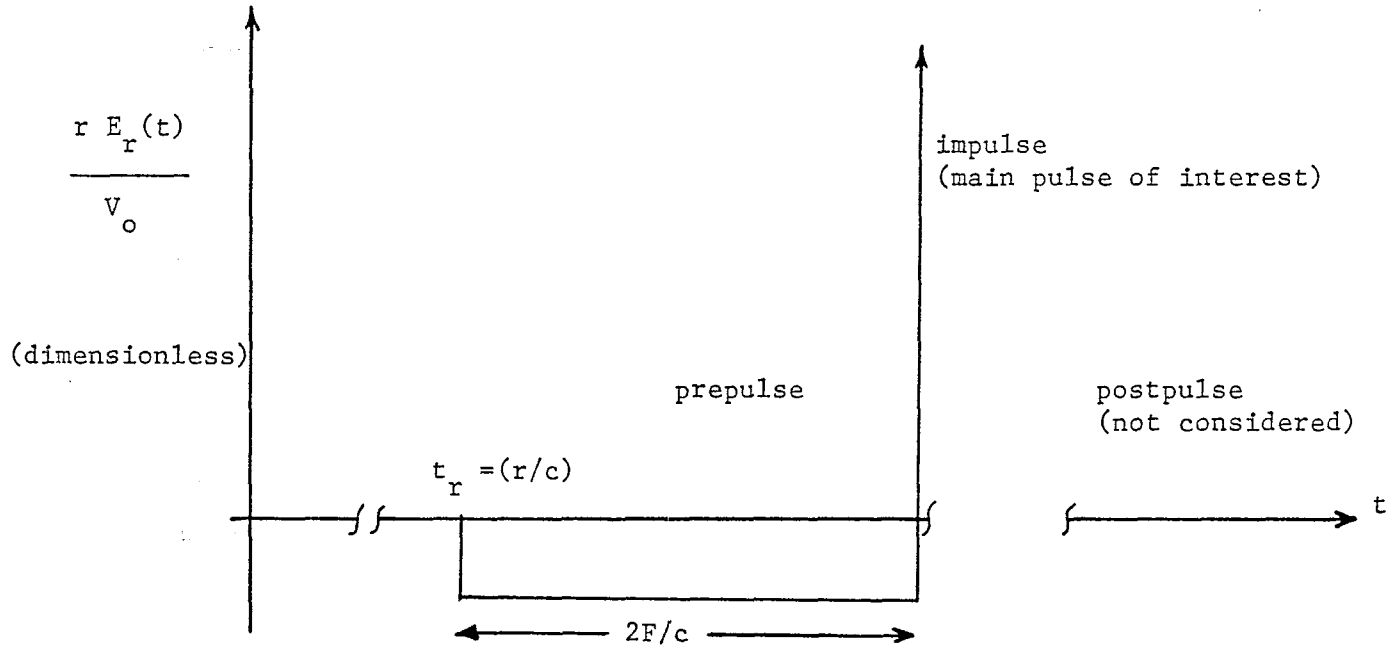

Figure 4. Far field on axis from an IRA fed by an ideal step function.

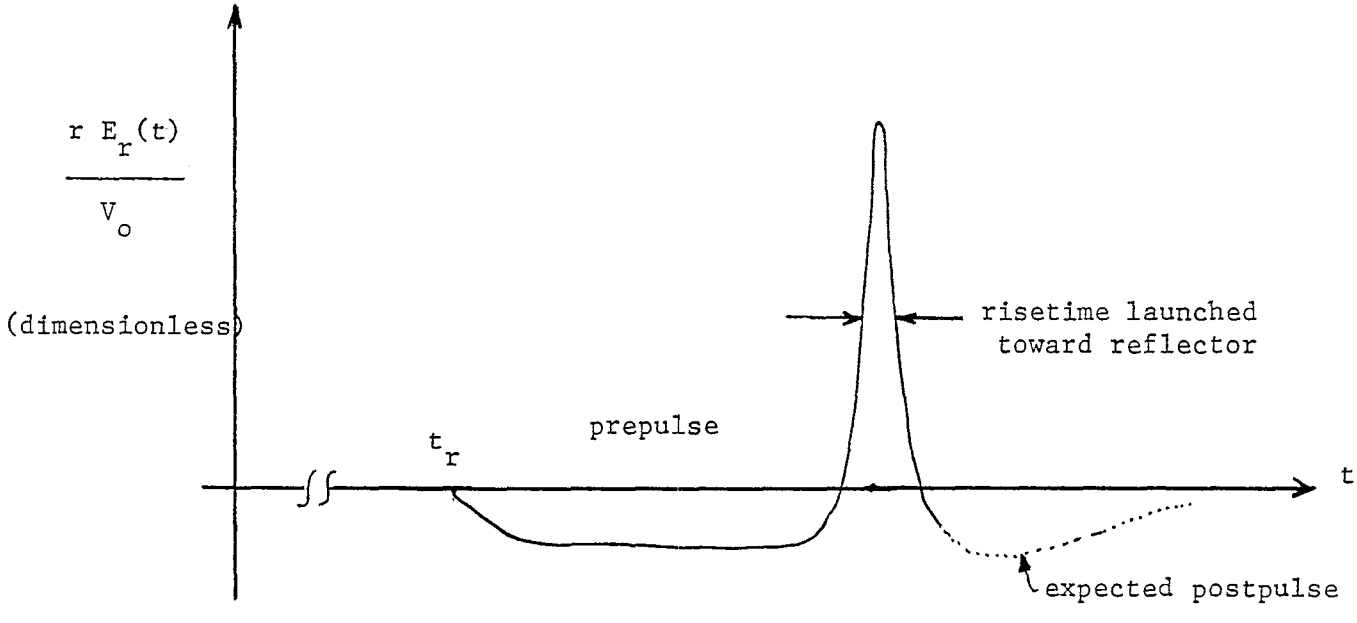

Figure 5. Far field on axis from an IRA fed by a fast-rising function.

The feed step is negative for the assumed signs of voltages on the launcher plates.

For one pair of narrow plates (plate width << plate separation) with applied voltages of $\left[\pm\frac{V_0}{2}u(t)\right]$, the feed step in the far field may be written as [5],

$$E_{y1}(r,\,t) = -\frac{V_0}{r}\,\frac{D}{4\pi f_g}\,\frac{1}{2F}\left[u(t-t_r) - u\left(t-\left(t_r+\frac{2F}{c}\right)\right)\right] \tag{1}$$

where

$V_0 \equiv$ potential difference between the two feed plates

$D \equiv$ diameter of the reflector = 2b

$f_g \equiv$ feed impedance/free space impedance

$F \equiv$ focal length

$c \equiv$ speed of light

The "exact" feed step amplitude, available in ((33) of [5]) is

$$-\frac{V_0}{r}\,\frac{1}{2K(m)\,\cot(\beta_2/2)} \tag{2a}$$

with $m = (b_1/b_2)^2$ and b_1, b_2 and β_2 are shown in Figure 1b. The above expression has simpler asymptotic forms for narrow plates ($(b_2/b_1) \rightarrow 1$) and wide plates ($(b_2/b_1) \rightarrow \infty$). The following expressions [5] are useful in evaluating the exact feed step amplitude in (2a) above. We specify $f_d = F/D$ and $f_g = Z_c^{(\mathrm{TEM})}/Z_0$ and then compute m, β_0, β_1 and β_2 using

$$\left.\begin{aligned} f_g &= K(m)/K'(m) \\ \beta_0 &= \arctan\left[\frac{1}{2f_d - 1/(8f_d)}\right] \\ \beta_1 &= 2\,\arctan\left[m^{1/4}\,\tan(\beta_0/2)\right] \\ \beta_2 &= 2\,\arctan\left[m^{-1/4}\,\tan(\beta_0/2)\right] \end{aligned}\right\} \tag{2b}$$

More importantly, the turn-off of the feed step occurs at $t = t_r + (2F/c)$ which can be explained as follows. Assuming a current flow of $\vec{J}(\vec{r},\,t)$ in retarded time on the plates, the feed step can be computed via,

$$\vec{E}_y(r,\,t) = \frac{\mu_0}{4\pi r}\overleftrightarrow{1}_z \cdot \frac{\partial}{\partial t}\int_V \vec{J}(\vec{r},\,t-(z/c))dV \tag{3}$$

For $t < (t_r + (2F/c))$, this integral must give the same answer as before. Assuming that the current $\vec{J}(\vec{r}, t)$ is perfectly terminated at reflector and is a step-function wave propagating on conical plates, for times larger than $(t_r + (2F/c))$, $\vec{J}$ is a constant and hence the time derivative vanishes and the feed step turns off. What happens at this instant is that the current $\vec{J}$ goes on to other parts of antennas and the integrals such as (3) give other terms e.g., main pulse, postpulse, etc. In the subscript for the radiated field on the left side of above equation, y refers to the y-component and the number following the y refers to the numbering scheme of the various temporal elements in the radiated field, as listed earlier (e.g., 1 refers to feed step).

2) *Impulse at* $t = [t_r + (2F/c)]$

The impulse-like radiation occurs at a time $t = [t_r + (2F/c)]$ for an observer location on axis. Recall that the switch center is located at $z = -z_s$ with $z = 0$ being the focal point or the launcher apex. Although the transient wave has to propagate a short distance in the oil medium of the lens, the design of the lens ensures that the wavefront outside the lens region is a sphere centered at the focal point. The impulse amplitude is given by [5],

$$E_{y2}(r, t) = \frac{V_0}{r} \frac{h_{a_y}}{2\pi c f_g} \delta\left(t - \left(t_r + \frac{2F}{c}\right)\right) \tag{4}$$

where the effective antenna height is given by [11],

$$h_{a_y} = \frac{\pi m^{-1/4}}{K(m)} b \left[1 - \frac{2}{\pi} \arcsin\left(\frac{1-\sqrt{m}}{1+\sqrt{m}}\right)\right] \tag{5}$$

Once again, the asymptotic forms are

$$E_{y2}(r, t) = \frac{V_0}{r} \frac{D}{4\pi c f_g} \delta\left(t - \left(t_r + \frac{2F}{c}\right)\right) \tag{6}$$

for narrow plates $(b_2/b_1) \rightarrow 1$ for which $h_{a_y} \simeq (D/2)$ (see Appendix C), and

$$E_{y2}(r, t) \simeq \frac{V_0}{r} \frac{D}{\pi^2 c} \delta\left(t - \left(t_r + \frac{2F}{c}\right)\right) \tag{7}$$

for wide plates for which

$$\left(\frac{b_2}{b} = \frac{b}{b_1}\right) \rightarrow \infty \quad ; \quad f_g \rightarrow 0$$
$$h_{a_y} = \left(\frac{2D}{\pi} f_g + \cdots\right) \quad \text{see Appendix C)} \tag{8}$$

One also notes that above expressions are the ideal results of a delta function radiator. The correct field is limited in amplitude by the aperture field with a small pulse width (replace δ by δ_a) to give the correct impulse or time integral [3].

3) *Feed-plate diffraction*

The diffraction from the feed plates may be classified into two parts. As the spherical TEM wave launched by the feed plates scatters off the paraboloidal surface, it encounters the plate edge and then the plates themselves. Consequently, the feed-plate diffraction occurs from the plate edge at the early time.

a) Plate edge diffraction

At early times when the finiteness of the plate edge is unobservable, this problem can be modelled by the classical diffraction from half-plane [7]. Keller and Blank [7] have treated a general problem of diffraction from a wedge, which can be simplified and specialized to a half-plane by making the wedge angle equal to zero. This solution is presented in Appendix A and the resultant far field on axis due to the diffraction from plate edge at early times is given by

$$E_{y3a}(r,\ t) = -\frac{V_0}{r}\ \frac{1}{\sqrt{\sin(\beta_1)}}\ \left(\frac{1}{\sqrt{2}\pi^2}\right)\left(\frac{2}{3}\right) \sqrt{\frac{2a}{ct-(r+2F)}}\ u\left(t-\frac{r}{c}-\frac{2F}{c}\right) \tag{9}$$

recalling that the source is turned on at $t = 0$ and the origin of coordinates is the focal point of the reflector, which is also the true apex of launcher plates. Strictly speaking, the above equation is asymptotically valid for a time less than (a/c) on average, after this diffraction process is initiated at a time $t = [t_r + (2F/c)]$.

b) Diffraction from the plates of finite width (<< wavelength)

For times larger than (a/c) and smaller than (b/c) so that, only the total current on plates is important, the scattered wave is diffracted from the plates. We can estimate this by modelling the plates by equivalent round conductors and quantifying the diffraction [8]. This solution is presented in Appendix B and the leading term in the resultant far field on axis due to the diffraction from the plates

(assumed to be 1 pair initially) is given by

$$E_{y3b}(r,\ t) \simeq -\frac{V_0}{r}\ \frac{1}{4\ \sin(\beta_0)}\ \frac{1}{\ell n\left[\frac{1}{\Gamma_e}\left\{\frac{2(ct-r)}{a_e\ \sin(\beta_0)}+1\right\}\right]}+\cdots \tag{10}$$

where

$a_e \equiv$ equivalent radius of the plates

$\Gamma_e \equiv$ exponential of Euler's constant $= 1.7810\cdots$

It should be remarked that we have estimated the diffraction from the plates in 2 time regimes. It is not clear how the two time regime solutions connect up. The diffraction from the launcher plates is of opposite sign compared to the impulse like radiation and initially falls off like $(1/\sqrt{t})$ and then asymptotically behaves like $(1/\ell n\sqrt{t})$.

4) *Diffracted fields from reflector edge*

Immediately following the impulse, one also has the diffracted signal from the circular rim of the parabolic reflector arriving at an observer on axis. We now estimate this edge diffracted signal.

The cross sectional view at $z = -z_r$ is shown in Figure 6. This is the plane in which the circular rim of the parabolic reflector is located. It is clear that in the $z = -z_r$ plane, the illuminating TEM fields are in the ϕ direction and hence parallel to the rim of the reflector. We look at the edge diffraction from one pair of plates (A-B) illustrated in Figure 6. The incident field illuminating the rim may be written as

$$\begin{aligned}
&\vec{E}^{(\mathrm{inc})}(\vec{r}',\ t) = E_\phi(\vec{r}',\ t)\quad \vec{1}_\phi \qquad \text{time domain}\\
&\tilde{\vec{E}}^{\mathrm{inc}}(\vec{r}',\ j\omega) = \tilde{E}_\phi(\vec{r}',\ j\omega)\quad \vec{1}_\phi \qquad \text{frequency domain}
\end{aligned} \tag{11}$$

The general far field expression for the edge diffraction in frequency domain is given by [9],

$$\begin{aligned}
\tilde{\vec{E}}_e(\vec{r},\ \omega) = \frac{e^{-jkr}}{4\pi r}\ \oint_{C_b}\Big[\vec{1}_\theta\Big(\tilde{E}_\theta^{(\mathrm{inc})}\,F_\theta\\
+\ Z_0\tilde{H}_\theta^{(\mathrm{inc})}\,G_\theta\Big)+\vec{1}_\phi\,\tilde{E}_\phi\,G_\phi\Big]\,e^{jk\vec{1}_r\cdot\vec{r}'}\,\mathrm{d}\ell
\end{aligned} \tag{12}$$

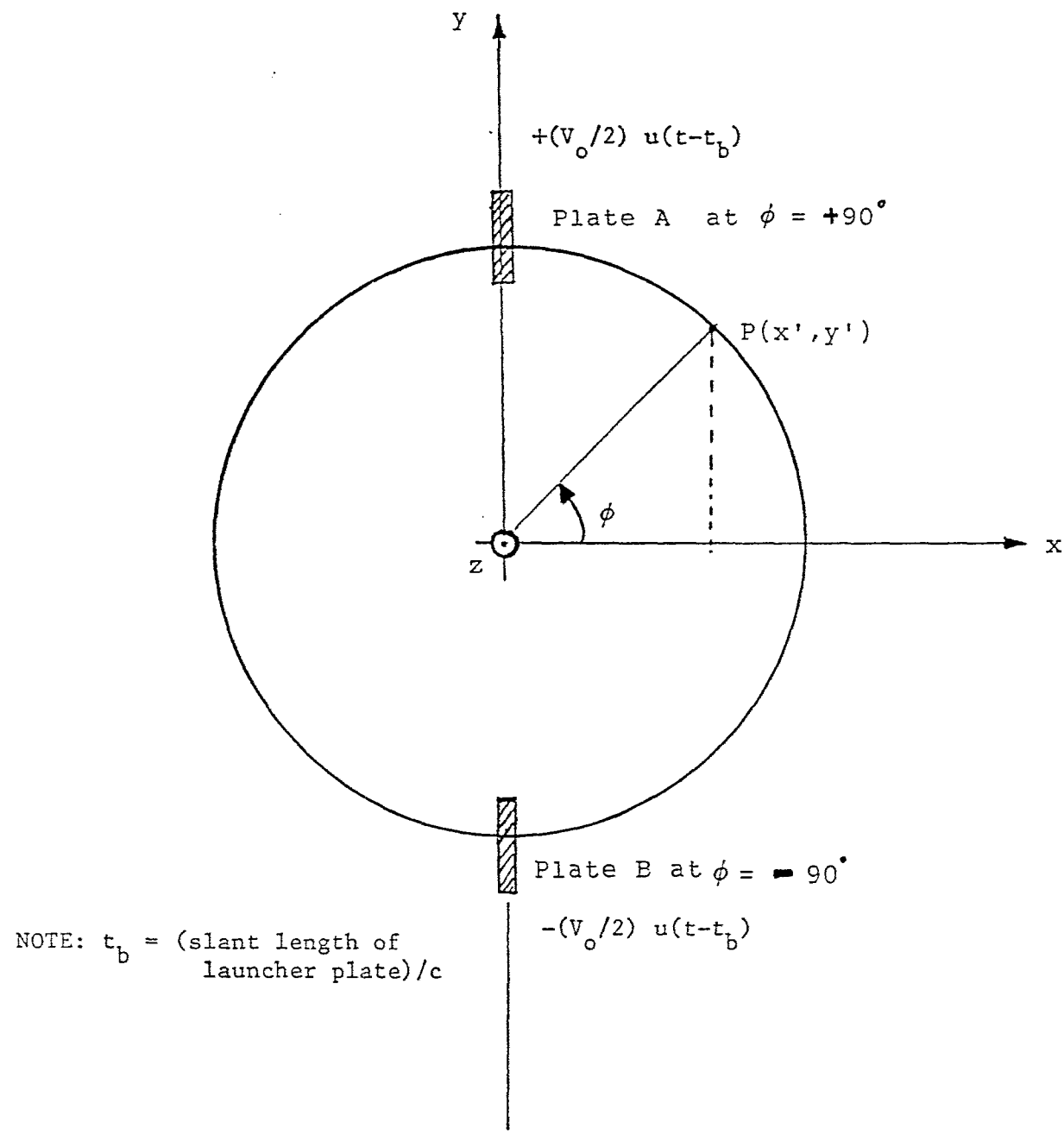

Figure 6. Circular rim of the reflector in the $z = -z_r$ plane.

where the one-dimensional integral is along the circular reflector edge. We now specialize the above equation for an observer on axis. The diffraction coefficients are given by [9]

$$-F_\theta = G_\phi = \frac{1-\sin(\beta_0/2)}{\cos(\beta_0/2)} = \tan\left(\frac{\pi-\beta_0}{4}\right) \qquad \text{and} \quad G_\theta = 0 \tag{13}$$

The vector $\vec{r}'$ denotes a point on the circular rim and for an observer on axis $\vec{1}_r = \vec{1}_z$ so that $e^{jk\vec{1}_r\cdot\vec{r}'} = e^{-jkz_r}$. Substituting, $\tilde{\vec{E}}_\theta^{(\text{inc})} = 0$ for TEM waves on self reciprocal apertures (Appendix B and [12]); $G_\theta = 0$, we have

$$\tilde{\vec{E}}_{y4}(\vec{r},\,\omega) = \frac{e^{-jk(r+z_r)}}{4\pi r}\, G_\phi \int_L \tilde{\vec{E}}^{(\text{inc})}(\vec{r}',\,\omega)\mathrm{d}\ell \tag{14}$$

we also know that for an observer on axis, there is no x-component of the rim diffracted field and consequently, we can consider the y-component of the above equation

$$\vec{1}_y \cdot \tilde{\vec{E}}_{y4}(\vec{r},\,\omega) = \tilde{\vec{E}}_{y4}(\vec{r},\,\omega) = -\frac{e^{-jk(r+z_r)}}{4\pi r}\, G_\phi \int_L \vec{1}_y \cdot \tilde{\vec{E}}^{(\text{inc})}\,\mathrm{d}\ell \tag{15}$$

or

$$\begin{aligned}
\tilde{E}_{y4} &= -\frac{e^{-jk(r+z_r)}}{4\pi r}\, G_\phi \oint_{C_b} \cos(\phi)\,\vec{E}_\phi\, e^{-jkr_0}\,\mathrm{d}\ell \\
&= -\frac{e^{-jk(r+z_r+r_0)}}{4\pi r}\, G_\phi \oint_{C_b} \tilde{E}_\phi\,\cos(\phi)\mathrm{d}\ell \\
&= -\frac{e^{-jk(r+2F)}}{4\pi r}\, G_\phi\, \xi_y
\end{aligned} \tag{16}$$

where the diffraction coefficient G_ϕ is given in (6) and ξ_y represents the integral

$$\xi_y = \oint_{C_b} \tilde{E}_\phi\,\cos(\phi)\mathrm{d}\ell = \oint_{C_b} \tilde{E}_y\,\mathrm{d}\ell \tag{17}$$

It is also noted that the negative sign in (15) and (16) represents the sign reversal when the incident field hits the metallic rim. The above integral is evaluated in Appendix C and is given by

$$\xi_y = -V_0\,\frac{\pi}{2}\,\frac{1}{m^{1/4}K(m)}\left[1-\frac{2}{\pi}\,\arcsin\left(\frac{1-\sqrt{m}}{1+\sqrt{m}}\right)\right] \tag{18}$$

where

$$K(m) \equiv \text{complete elliptic function of the first kind}$$

$$m \equiv \text{parameter} = (b_1/b_2)^2 \quad \text{(see Figure 6b)}$$

It has been verified that the ξ_y expression of (18) is consistent with asymptotic results obtained for narrow and wide plates. Substituting (18) into (16) and taking the inverse transform, we have

$$E_{y4}(r,\, t) = \frac{V_0}{4\pi r}\left(\frac{\pi}{2}\right)\frac{1-\sin(\beta_0/2)}{\cos(\beta_0/2)}\frac{1}{m^{1/4}K(m)} \left[1-\frac{2}{\pi}\arcsin\left(\frac{1-\sqrt{m}}{1+\sqrt{m}}\right)\right] u\left(t-\frac{r}{c}-\frac{2F}{c}\right) \tag{19}$$

The above expression is the leading term in y-directed rim-diffracted field on axis, at a distance r from the focal point for the case of one pair of coplanar plates (see Figure 6). It is noted that the above expression is asymptotically exact, since we have used the exact TEM incident field (ϕ-directed) which is parallel to the circular rim of the reflector. This result is a step function in an early-time sense.

5) *Constraints on entire pulse*

The radiation at low frequencies may be characterized by a set of electric and magnetic dipole moments. Let us denote these late-time dipole moments by $\vec{p}(t)$ and $\vec{m}(t)$ respectively. With reference to Figure 6, it is observed that the $\vec{p}(t)$ [10] is oriented along $\vec{1}_y$ and $\vec{m}(t)$ is oriented along $-\vec{1}_x$ direction so that the resultant radiation is along $\vec{1}_y \times (-\vec{1}_x)$ or $\vec{1}_z$ direction. The low-frequency radiation pattern from this pair of balanced ($|\vec{m}| = c|\vec{p}|$) dipole moments is $(1 + \cos(\theta))$ where θ is the polar angle measured from the $+z$ axis. It is noted that the $-z$ axis behind the reflector is a direction of null ($\theta = \pm\pi$) for the low-frequency radiation. This physical fact can be used in the experimental balancing of the two dipole moments by varying the terminating impedances at the junction of the feed plates and the reflector rim. For example, increasing the terminating impedance in the loop over the value of the characteristic impedance $Z_c^{(\mathrm{TEM})}$ would lower the loop current and hence lower the magnetic dipole moment.

One can summarize the constraints on the entire radiated pulse [13, 14] by observing: (i) that the complete time integral of the radiated waveform must be

zero and (ii) the low-frequency radiation is proportional to $\vec{p}(\infty)$ or $\vec{m}(\infty)$ which are the late-time dipole moments. The constraints on $\vec{E}_f$ are given below

$$\int_{-\infty}^{\infty} \vec{E}_f(r,\, t)dt = 0 \tag{20a}$$

$$\int_{-\infty}^{\infty} \int_{-\infty}^{t} \vec{E}_f(r,\, t')\, dt'\, dt = -\frac{\mu_0}{4\pi r} \left[\vec{p}(\infty) - \frac{\vec{1}_z}{c} \times \vec{m}(\infty)\right] \tag{20b}$$

As noted earlier, for properly terminated TEM lines, the low-frequency radiation pattern associated with the dipole moments is a cardioid with its maximum along the boresight and a null in the backward direction.

Gathering various temporal elements of the boresight radiation discussed above, one arrives at Figure 7 for the far field from a reflector IRA fed by one set of coplanar plates. The IRA under discussion is illustrated at the top of Figure 7, and the y-directed far field (normalized) at the bottom. The practical switch at $z = -z_s$ closes at $t = t_1$ as mentioned earlier, which in effect turns on an ideal source at $t = 0$ at the apex. Under this assumption, the feed step for an on-axis observer starts at $t = t_r = r/c$. The feed step is negative, while the impulse 2 is positive. The feed plate diffraction is negative (3a and 3b) while the rim diffraction 4 is positive. The results can be expressed as

$$\begin{aligned}
&\vec{E}_f(\vec{r},\, t) = \vec{1}_y\, E_y(r,\, t) \\
&E_y(r,\, t) = E_{y1}(r,\, t) + E_{y2}(r,\, t) + E_{y3}(r,\, t) + E_{y4}(r,\, t) \\
&\qquad\qquad + \text{ low-frequency radiation from dipole} \\
&\qquad\qquad \text{moments resulting in time integral} \\
&\qquad\qquad \text{constraints on entire pulse}
\end{aligned} \tag{21}$$

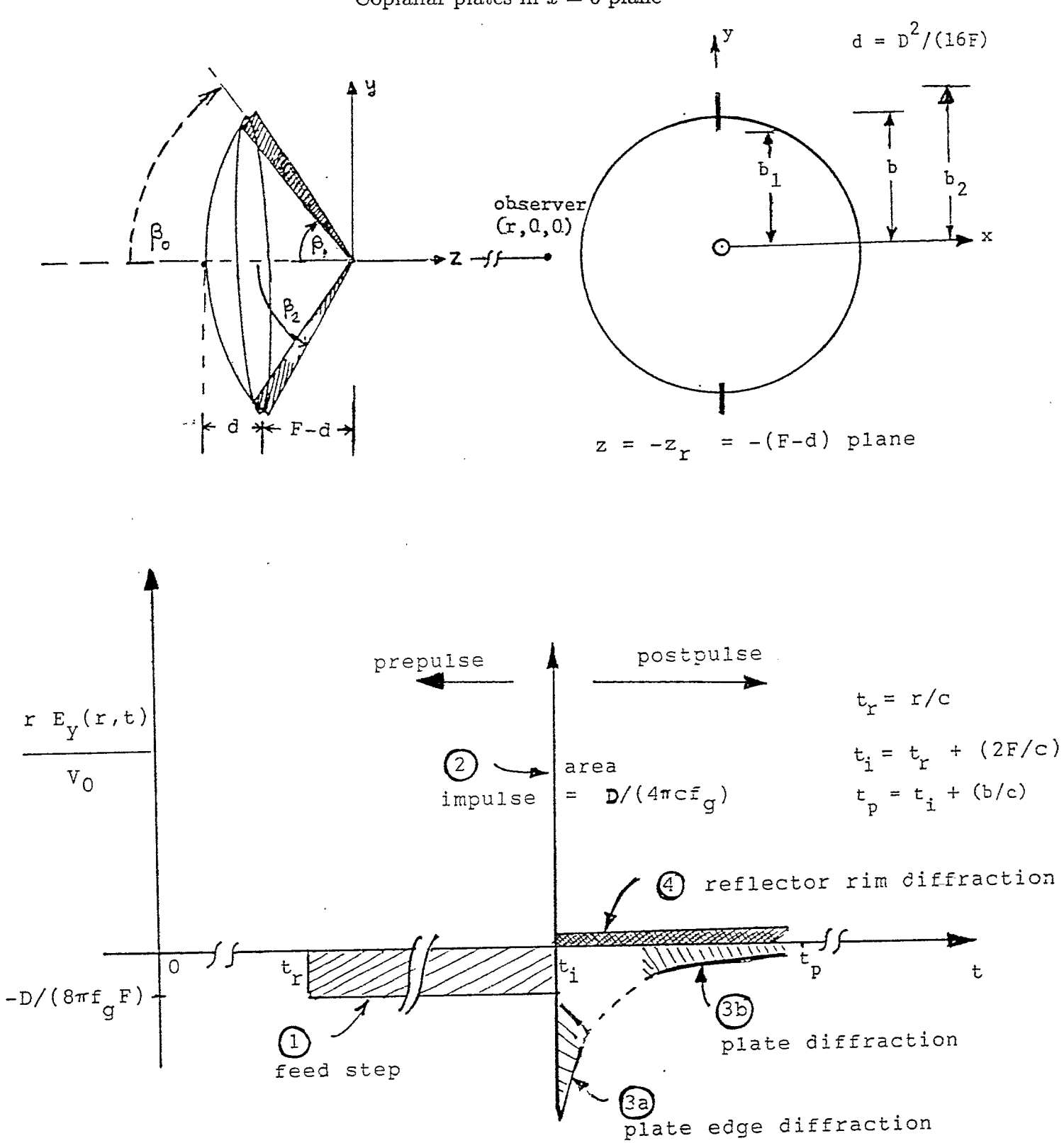

Figure 7. On-axis radiation from a canonical IRA illustrated at the top.

where

$E_{y1}(r,\, t) \equiv$ feed step $\equiv$ prepulse

$$\simeq -\frac{V_0}{r}\ \frac{1}{2K(m)\cot(\beta_2/2)}\ \left[u\Big(t-\frac{r}{c}\Big)-u\Big(t-\frac{r}{c}-\frac{2F}{c}\Big)\right]$$
$$\simeq -\frac{V_0}{r}\ \frac{D}{4\pi f_g}\ \frac{1}{2F}\left[u\left(t-\frac{r}{c}\right)-u\Big(t-\frac{r}{c}-\frac{2F}{c}\Big)\right] \qquad (22)$$
(for narrow plates with width << separation)

$E_{y2}(r,\, t) \equiv$ Impulse

$$= \frac{V_0}{r}\ \frac{h_{a_y}}{2\pi c f_g}\ \delta\Big(t-\frac{r}{c}-\frac{2F}{c}\Big)$$
$$\simeq \frac{V_0}{r}\ \frac{D}{4\pi c f_g}\ \delta\Big(t-\frac{r}{c}-\frac{2F}{c}\Big) \qquad (23)$$
(for narrow plates with width << separation)

$E_{y3a}(r,\, t) \equiv$ plate-edge diffraction

$$\simeq -\frac{V_0}{r}\ \frac{1}{\sqrt{\sin(\beta_1)}}\ \left(\frac{1}{\sqrt{2}\,\pi^2}\right)\left(\frac{2}{3}\right)\sqrt{\frac{2a}{ct-(r+2F)}}$$
$$u\left(t-\frac{r}{c}-\frac{2F}{c}\right) \qquad (24)$$
(see Appendix A for the approximations in above)

$E_{y3b}(r,\, t) \equiv$ plate diffraction (round conductor approx.)

$$\simeq -\frac{V_0}{r}\ \frac{1}{4\,\sin(\beta_0)}\ \frac{1}{\ell n\left[\frac{1}{\Gamma_e}\left\{\frac{2(ct-r)}{a_e\,\sin(\beta_0)}+1\right\}\right]} \qquad (25)$$
(see Appendix B for the approximations in above)

$$E_{y4}(r,\, t) \equiv \text{diffraction from the circular rim of the reflector}$$

$$\simeq \frac{V_0}{4\pi r}\left(\frac{\pi}{2}\right)\frac{1-\sin(\beta_0/2)}{\cos(\beta_0/2)}\frac{1}{m^{1/4}K(m)} \left[1-\frac{2}{\pi}\arcsin\left(\frac{1-\sqrt{m}}{1+\sqrt{m}}\right)\right] u\left(t-\frac{r}{c}-\frac{2F}{c}\right) \tag{26}$$

In addition to the prepulse, pulse of main interest and the post pulse listed above, one also recognizes the constraints on the entire radiated waveform in the form of time integrals. These constraints were discussed earlier and require that the first time-integral of the entire pulse be zero and the second time-integral be proportional to late-time dipole moment of the IRA.

Recall that the radiated field outlined above is for a step function $u(t)$ excitation. In practical situations, one never has an ideal step function and so $u(t)$ may be replaced by a general $f(t)$ and $\delta(t)$ in (23) then becomes $(\partial f/\partial t)$. Examples of $f(t)$ are:

a)

$$f_1(t) = u(t)[1-e^{-\alpha t}] \tag{27}$$

$$\equiv \text{fast-rising "step function"}$$

for which the impulse $\delta(t)$ would be replaced by $(\partial f_1/\partial t)$

b)

$$f_2(t) = (e^{-\beta t}-e^{-\alpha t})u(t) \qquad \text{with} \quad \alpha \gg \beta \tag{28}$$

$$\equiv \text{fast-rising, slowly decaying "double-exponential" function}$$

for which the impulse $\delta(t)$ would be replaced by $(\partial f_2/\partial t)$.

The leading terms of the time-domain radiated field on axis described above are useful in the design and evaluation of IRAs of this type. A prototype IRA is under construction and its measured performance data may be compared with the expressions in this note, at a later date.

III. Summary

In this note, the past analyses of the on-axis radiation from reflector IRAs are extended to include the diffraction from the feed plates as well as the circular rim of the reflector. Leading terms of these diffracted signals in time-domain are obtained in closed form, under the assumption of a step function excitation. We recall that the feed step (or prepulse) is a negative going step with a duration of $(2F/c)$. The impulse is of the opposite sign. The amplitude of the feed step and also the area under the impulse are known from past analyses. In this note, we have obtained the leading terms for diffractions from the plate edge, plate(s) and the reflector rim. The diffraction from the plate edge is based on a classical half-plane solution valid at early times. The diffraction from the plates are obtained by estimating the diffraction from an equivalent cylindrical conductor. The diffraction from the circular reflector rim is obtained accurately since the incident field on the rim is well known from the spherical TEM wave propagating on the feed plates.

The radiated waveform is decomposed into prepulse, main pulse and postpulse. The postpulse is seen to consist of plate edge diffraction (3a), diffraction from plate of width << wavelength (3b) and the rim diffraction (4). The formulas derived for (3a) and (3b) can be improved by evaluating integrals over non-uniform E_y incidence, perhaps numerically. The rim diffraction (4) on the other hand is asymptotically exact and appears to be complete.

It is noted that at low frequencies one can characterize the radiated field from a set of electric and magnetic dipole moments which results in certain constraints on time integrals of the entire radiated waveform. Essentially, the complete first-time integral of the radiated waveform must be zero and the second-time integral must be proportional to the late-time dipole moment. Formally, this analysis completes all aspects of the radiated fields on axis from reflector IRAs. The results obtained here are useful in designing and evaluating the performance of this type of IRA.

APPENDIX A

Plate Edge Diffraction

We start with the Keller and Blank [7] formulation for the diffraction from a wedge and specialize it to a half plane. With reference to Figure 8, the incident field is given by

$$Z_0\vec{H}^{(\mathrm{inc})} = \vec{1}_1 \times \vec{E}^{(\mathrm{inc})} = \vec{1}_i \times \vec{1}_z \; E_0 \; u\left(t - \frac{\vec{1}_1 \cdot \vec{r}}{c}\right) \tag{29}$$

The rectangular coordinate system (x, y, z) indicated in Figure 8 is for the purposes of this Appendix only. It should not to be confused with the coordinate system in Sections I and II. The approach is as follows. For the given incident field, one finds the diffracted/scattered field everywhere from which the current induced on the metallic conductors may be found. By integrating these currents, one gets the radiated field.

Keller and Blank [7] compute the diffracted fields via a computation of the electric potential function U, also indicated in Figure 8. We can specialize the potential function (Equation 16 of [7]) to the case of $\phi_1 = 0$ and $\phi_0 = 0$ to get the potential function for diffraction from a half-plane. Letting $\phi_1 = 0$ and $\phi_0 = 0$, we have the potential function given by

$$U = 1 - \frac{2}{\pi} \arctan\left\{\frac{(1-\rho)}{2\rho^{1/2}\cos\left(\dfrac{\phi-\pi}{2}\right)}\right\} \tag{30}$$

The values for the potential u ranges from 0 to 1 and the (arctan) values go from 0 to $(\pi/2)$. In the above expression,

$$\rho = \frac{\Psi}{ct + (c^2t^2 - \Psi^2)^{1/2}} = e^{-\mathrm{arccosh}(ct/\Psi)} \tag{31}$$

where Ψ is the cylindrical radius. Substituting (31) into (30), the potential function becomes

$$U(\Psi, \phi) = 1 - \frac{2}{\pi} \arctan\left\{\left[\frac{\dfrac{ct}{\Psi} - 1}{2}\right]^{1/2} \cos^{-1}\left(\frac{\phi-\pi}{2}\right)\right\} \tag{32}$$

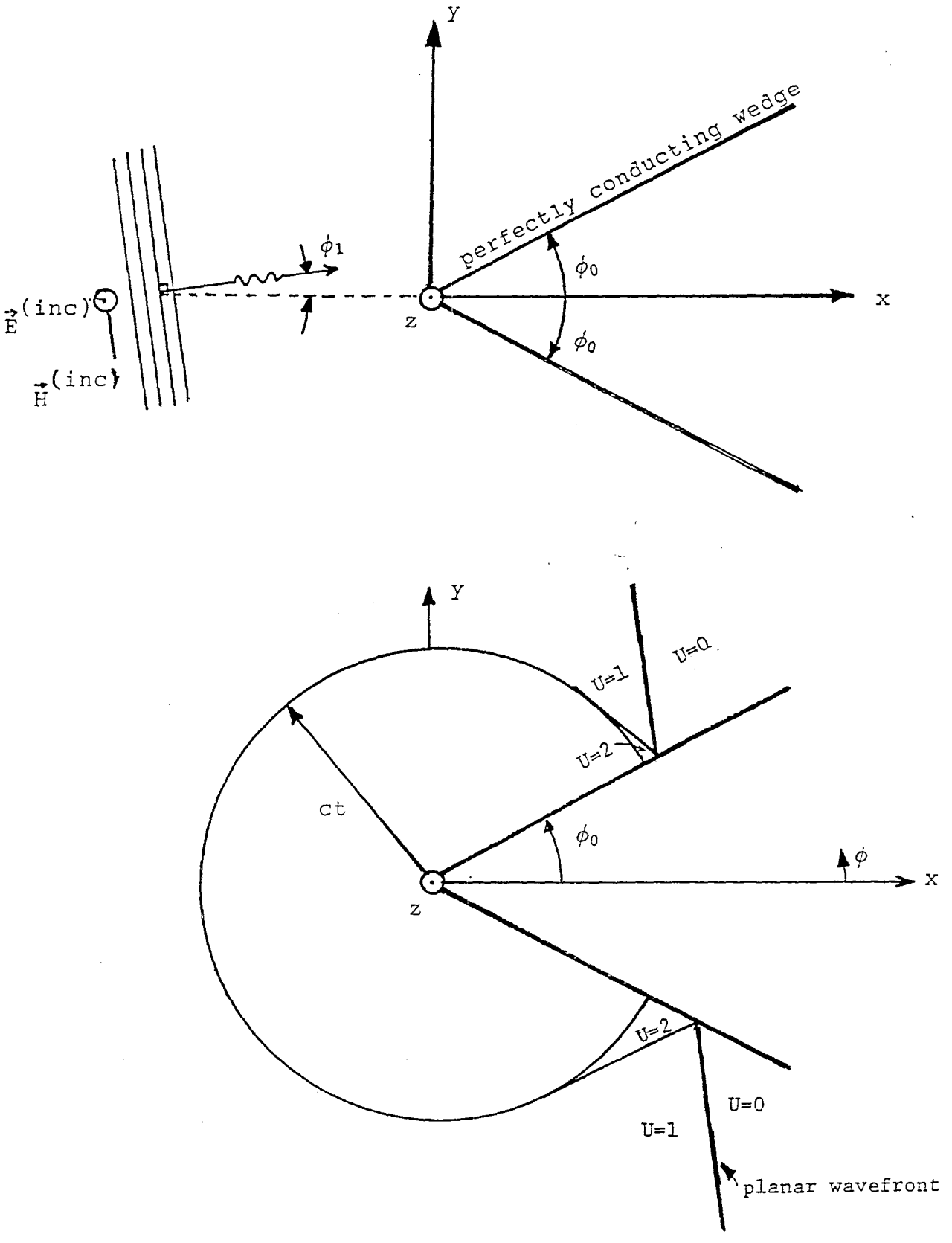

Figure 8. Diffraction from a wedge[7] (we let $\phi_1 \to 0$ and $\phi_0 \to 0$)

with $(ct/\Psi) > 1$ and $|\phi - \pi| < \pi$.

We now observe that if the incidence were not normal as in Figure 8, but off normal at an angle θ_i, the incident field amplitude in (29) is now $E_0 \sin(\theta_i)$ in place of E_0. For present purposes θ_i is taken as the leading edge in this edge diffraction and therefore $\theta_i = \beta_1$ and β_2 does not enter this formulation. The diffracted electric and magnetic fields in cartesian coordinates are given by [15]

$$\vec{E} = -c\cot(\theta_i)\int_{-\infty}^{t}\left[\frac{\partial U}{\partial x}\,\vec{1}_x + \frac{\partial u}{\partial y}\,\vec{1}_y\right]dt + U\,\sin(\theta_i)\,\vec{1}_z \tag{33}$$

$$Z_0\,\vec{H} = -\frac{c}{\sin(\theta_i)}\int_{-\infty}^{t}\left[\frac{\partial U}{\partial y}\,\vec{1}_x - \frac{\partial U}{\partial x}\,\vec{1}_y\right]dt \tag{34}$$

To find the currents induced the x-component of the magnetic field is the interesting quantity and, it is given by

$$Z_0\frac{\partial H_x}{\partial t} = -\frac{c}{\sin(\theta_i)}\,\frac{\partial U}{\partial y} \tag{35}$$

or

$$\frac{Z_0}{\sin(\theta_i)}\,\frac{\partial H_x}{\partial\left(\dfrac{t}{\sin(\theta_i)}\right)} = -\frac{c}{\sin\theta_i}\,\frac{\partial}{\partial y}\,U\left(x,\,y,\,\frac{t}{\sin(\theta_i)}\right) \tag{36}$$

The sheet current $\vec{J}_s$ is given by

$$\vec{J}_s = J_s\,\vec{1}_z = \vec{1}_z\left[-H_\Psi\,|_{x=0+} + H_\Psi|_{x=0-}\right] \tag{37}$$

Using (32) in (34), the sheet current becomes

$$\vec{J}_s = \vec{1}_z\,\frac{E_0}{Z_0}\,\frac{4\sqrt{2}}{\pi}\left[\left(\frac{ct}{x\,\sin(\theta_i)}\right) - 1\right]^{1/2} \quad \text{for } z = 0 \tag{38}$$

For a general value of z, we have

$$\vec{J}_s = \vec{1}_z\,\frac{E_0}{Z_0}\,\frac{4\sqrt{2}}{\pi}\left[\frac{\dfrac{ct}{x} + \dfrac{z}{x}\cos(\theta_i)}{\sin(\theta_i)} - 1\right]^{1/2} u\left(\frac{ct}{x}\right) \tag{39}$$

Figure 9 shows a strip of constant width Ψ_0, the angle of incidence θ_i and the direction of current flow along the z-axis. Knowing the sheet current, the far field is given by

$$\vec{E}_f\left(r,\,t + \frac{\vec{1}_1\cdot\vec{r}}{c}\right) = -\frac{\mu_0\ell}{4\pi r}\,\frac{\partial}{\partial t}\int_0^{r_0}\sin(\theta_i)\,\vec{1}_p\,J_s\left(x',\,z',\,t + \frac{\vec{1}_1\cdot\vec{r}}{c}\right)dr' \tag{40}$$

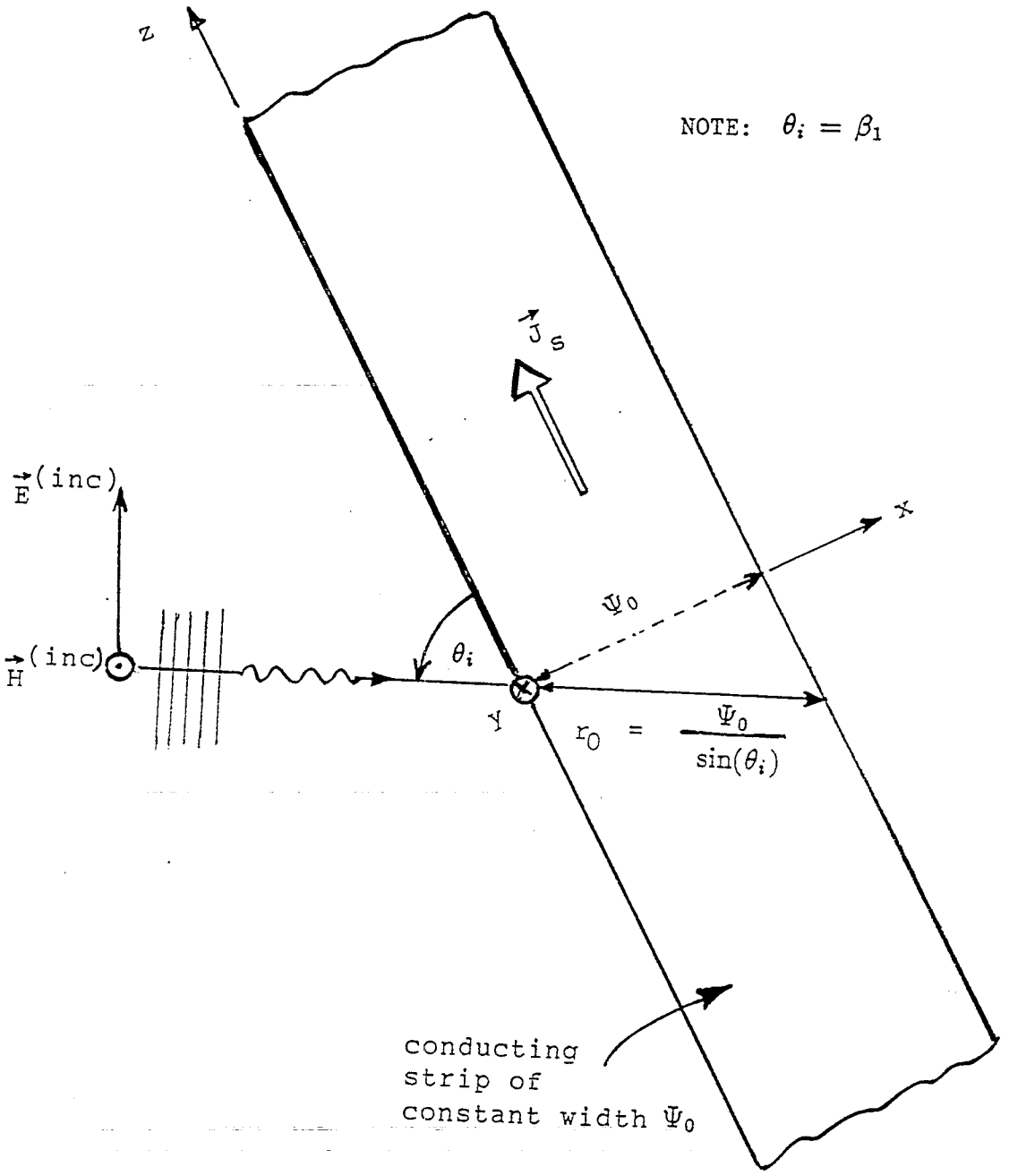

Figure 9. Geometry of sheet current flow w.r.t. the incident field.

Substituting for $\vec{J}_s$ from (38), we have on axis

$$\vec{E}_f\left(r, t+\frac{r}{c}\right) = -\frac{\mu_0}{4\pi r}\,\ell\,\sin(\theta_i)\,\vec{1}_p\,\frac{\partial}{\partial t} \int_0^{r_0}\left[\frac{E_0}{Z_0}\,\frac{4\sqrt{2}}{\pi}\right]\left[\frac{ct}{x'\sin(\theta_i)}\right]^{1/2} dr' \tag{41}$$

Using $(\mu_0/Z_0) = c^{-1}$ and $dr' = dx'/\sin(\theta_i)$,

$$\vec{E}_f\left(r, t+\frac{r}{c}\right) = -\frac{E_0\ell}{4\pi r}\,\frac{4\sqrt{2}}{\pi}\,\frac{1}{\sqrt{\sin(\theta_i)}}\,\vec{1}_p\left[\frac{\Psi_0}{ct-r}\right]^{1/2} u(ct-r) \tag{42}$$

$$\begin{aligned} &\vec{1}_p \equiv \text{polarization of the e-field} \\ &\ell = b_1 \quad ; \quad E_0 \simeq \frac{V_0}{2b_1} \quad \text{on average} \end{aligned} \tag{43}$$

while Ψ_0 is a position dependent plate width with minimum and maximum values of 0 and $2a$ respectively, the average value of $\sqrt{\Psi_0}$ in above is given by

$$\sqrt{\Psi_0}\Big|_{\text{average}} = \frac{1}{\ell}\int_0^{\ell}\sqrt{2a\left(\frac{y}{\ell}\right)}\,dy = \frac{2}{3}\sqrt{2a} = \sqrt{\frac{8a}{9}} \tag{44}$$

So, to a first order

$$\vec{E}_f\left(r, t+\frac{r}{c}\right) = -\frac{V_0}{r}\,\frac{1}{\sqrt{\sin(\theta_i)}} \vec{1}_p\left(\frac{1}{\sqrt{2}\pi^2}\right)\left(\frac{2}{3}\right)\sqrt{\frac{2a}{ct-r}}\,u(ct-r) \tag{45}$$

This expression is asymptotically valid for a time less than (Ψ_0/c) or (a/c) after diffraction process is initiated at $t = [t_r + (2F/c)]$, noting that an average value of Ψ_0 is a. As noted earlier, we can use $\theta_i = \beta_1$ [see (2b)] for numerical computations. Substituting a more accurate y-dependent expression for the incident field (E_0 replaced by $E_y^{(\text{inc})}(y)$) could lead to more accurate results in the future.

APPENDIX B

Diffraction from the Plates of Finite Width (<< Wavelength)

The diffraction from the plates may be modelled by considering an equivalent problem of diffraction from a cylinder. The cylinder has an effective radius a_e which can be approximated to be (1/4) of plate width [16]. The maximum plate width is 2a so that the maximum value of $a_e = (a/2)$. The geometry of the model problem is shown in Figure 10. Once again, the rectangular coordinate system (x, y, z) indicated in Figure 10 is for the purposes of this Appendix only. It should not be confused with the coordinate system in Sections I and II. We follow the analysis of [8] and define a normalized time

$$q^* = \left[\frac{ct}{a_e \sin(\theta_i)} + 1\right] \tag{46}$$

So that the induced current is zero for negative values of q^*. Note that the incidence angle θ_i is well approximated by β_0 of (2b). Let us denote the incident field by

$$\vec{E}^{(\text{inc})} = E_0 \ \vec{1}_p \ u\left(t - \frac{\vec{1}_1 \cdot \vec{r}}{c}\right) \tag{47}$$

Using the results of [8] which is for an impulse excitation, for our step-function excitation, we have

$$I(t) = \int_{-\infty}^{q^*} \frac{2\pi a_e}{Z_0} \ E_0 \ F(q^*) dq^* \tag{48}$$

or

$$\frac{\partial I(t)}{\partial t} = \frac{1}{t_0} \ \frac{2\pi a_e}{Z_0} \ E_0 \ F(q^*) \tag{49}$$

where

$$t_0 \simeq \frac{a_e \ \sin(\theta_i)}{c}$$

$$F(q^*) = \frac{1}{\ell n\left(\frac{2q^*}{\Gamma_e}\right)} \tag{50}$$

$$\Gamma_e = 1.7810\ldots \equiv \text{exponential of Euler's constant}$$

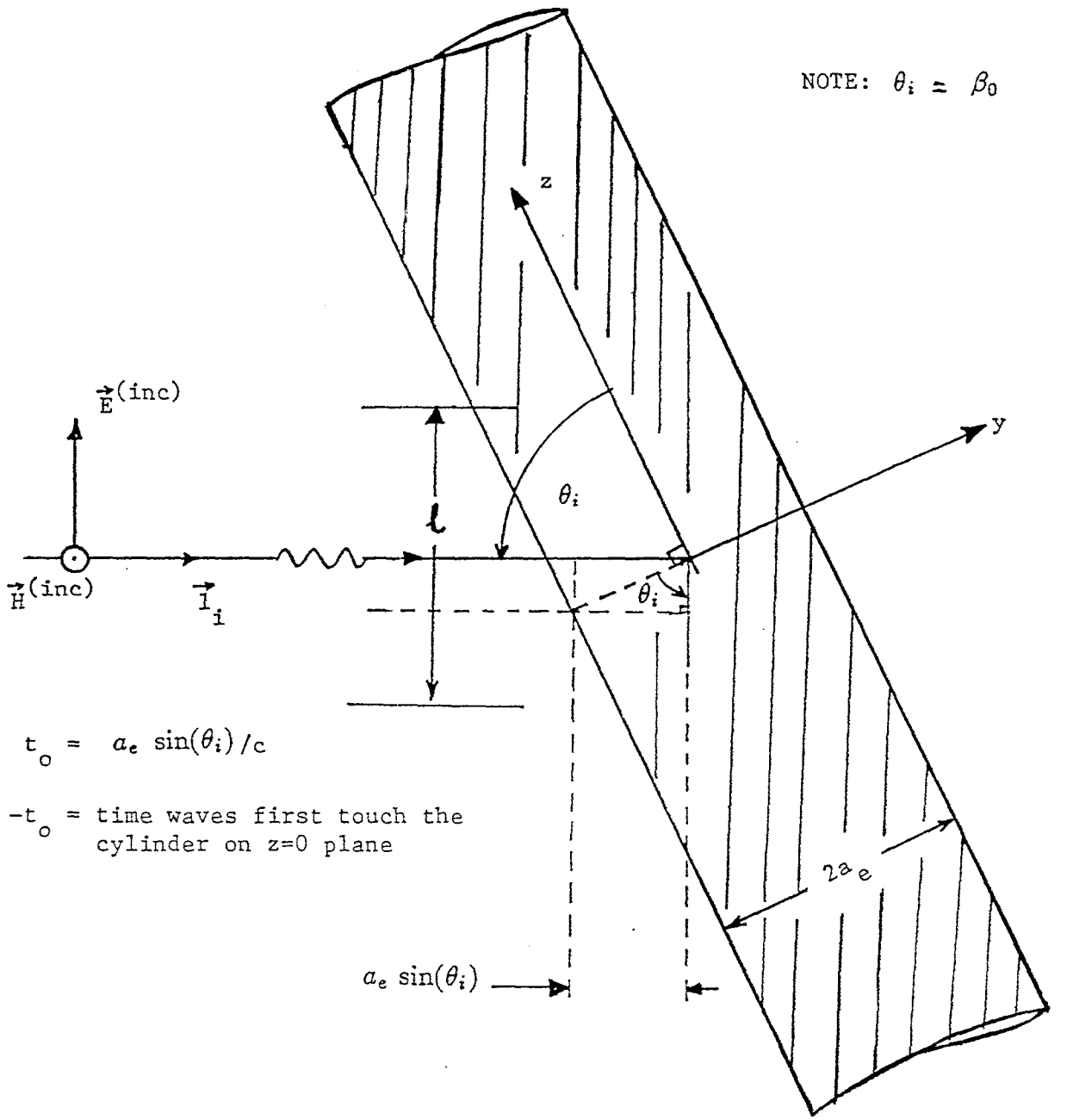

Figure 10. Geometry of diffraction from a cylindrical conductor.

We can now evaluate the far field from the knowledge of the current flow as follows

$$\vec{E}_f\left(\vec{r},\, t+\frac{\vec{1}_1\cdot\vec{r}}{c}\right) = -\frac{\mu_0}{4\pi r}\,\frac{\partial}{\partial t}\left\{\vec{1}_p\,(\sin(\theta_i))\int_{\text{length}} I\left(t-\frac{r}{c}\right)d\ell\right\}$$
$$= -\frac{\mu_0}{4\pi r}\,\vec{1}_p\,\ell\,\frac{\partial I(t)}{\partial t} \tag{51}$$

Substituting for $(\partial I/\partial t)$ from (49), we have

$$\vec{E}_f(r,\, t) = -\frac{E_0\ell}{2r\,\sin(\theta_i)}\,\ell n^{-1}\left[\frac{1}{\Gamma_e}\left\{\frac{2(ct-r)}{a_e\sin(\theta_i)}+1\right\}\right] \tag{52}$$

Once again, an average value of $E_0 \simeq V_0/(2b_1)$ and $\ell \simeq b_1$, which reduces (52) to

$$\vec{E}_f(r,\, t) \simeq -\frac{V_0}{4r}\,\frac{1}{\sin(\theta_i)}\,\ell n^{-1}\left[\frac{1}{\Gamma_e}\left\{\frac{2(ct-r)}{a_e\,\sin(\theta_i)}+1\right\}\right]+\cdots \tag{53}$$

As we remarked earlier, the incidence angle θ_i in above may be replaced by β_0 found in (2b). Once again as in the previous appendix, using more accurate, position dependent incident field $E_y^{(\text{inc})}(y,\, t)$ in (48) could lead to more accurate results in the future.

APPENDIX C

Diffraction from the Reflector Rim

[Evaluation of ξ_y in (17)]

Equation (17) is reproduced below

$$\xi_y = \oint_{C_b} \tilde{E}_\phi \cos(\phi) d\ell = \oint_{C_b} \tilde{E}_y \, d\ell = \oint_{C_{br}} 2\tilde{E}_y \, d\ell \tag{54}$$

This applies to contour C_b on the circle of radius b with the incident electric field parallel to C_b ($= C_{br} \cup C_{bl}$). These contours are shown in Figure 11. In general

$$\xi = \int_{C_b} \vec{E} d\ell = \xi_x \, \vec{1}_x + \xi_y \, \vec{1}_y \qquad \text{or} \qquad \xi = \int_{C_b} E d\ell = \xi_x - j\xi_y \tag{55}$$

Substituting

$$E = E_x - jE_y = -\frac{V_0}{\Delta u} \frac{dw(\xi)}{d\xi}, \tag{56}$$

$$\begin{aligned} \xi &= 2 \int_{C_{br}} E d\ell = -\frac{2V_0}{\Delta u} \int_{C_{br}} \frac{dw(\xi)}{d\xi} \, d\ell \\ &= j \frac{2V_0}{\Delta u} \int_{-\pi/2}^{\pi/2} \frac{dw}{d\phi} e^{-j\phi} \, d\phi \end{aligned} \tag{57}$$

Integrating by parts,

$$\xi = j \frac{2V_0}{\Delta u} \left\{ we^{-j\phi} \Big|_{-\pi/2}^{\pi/2} + j \int_{-\pi/2}^{\pi/2} we^{-j\phi} \, d\phi \right\} \tag{58}$$

Noting $\left| we^{-j\phi} \right|_{-\pi/2}^{\pi/2} = u_+(-j) - u_-(-j) + jv(-j) - jv(j) = -K(m_1)$

$$\xi = -\frac{2V}{\Delta u} \left\{ \int_{-\pi/2}^{\pi/2} we^{-j\phi} d\phi + jK(m_1) \right\} \tag{59}$$

Using $w = u + jv$ and considering

$$\int_{-\pi/2}^{\pi/2} v \, e^{-j\phi} d\phi = -\frac{1}{2} \; K(m_1) j e^{-j\phi} \Big|_{-\pi/2}^{\pi/2} = -K(m_1) \tag{60}$$

So,

$$\xi = -\frac{2V_0}{\Delta u} \int_{-\pi/2}^{\pi/2} u \, e^{j\phi} d\phi = j \frac{2V_0}{\Delta u} \frac{1}{b} \int_{C_{br}} u d\xi^* \tag{61}$$

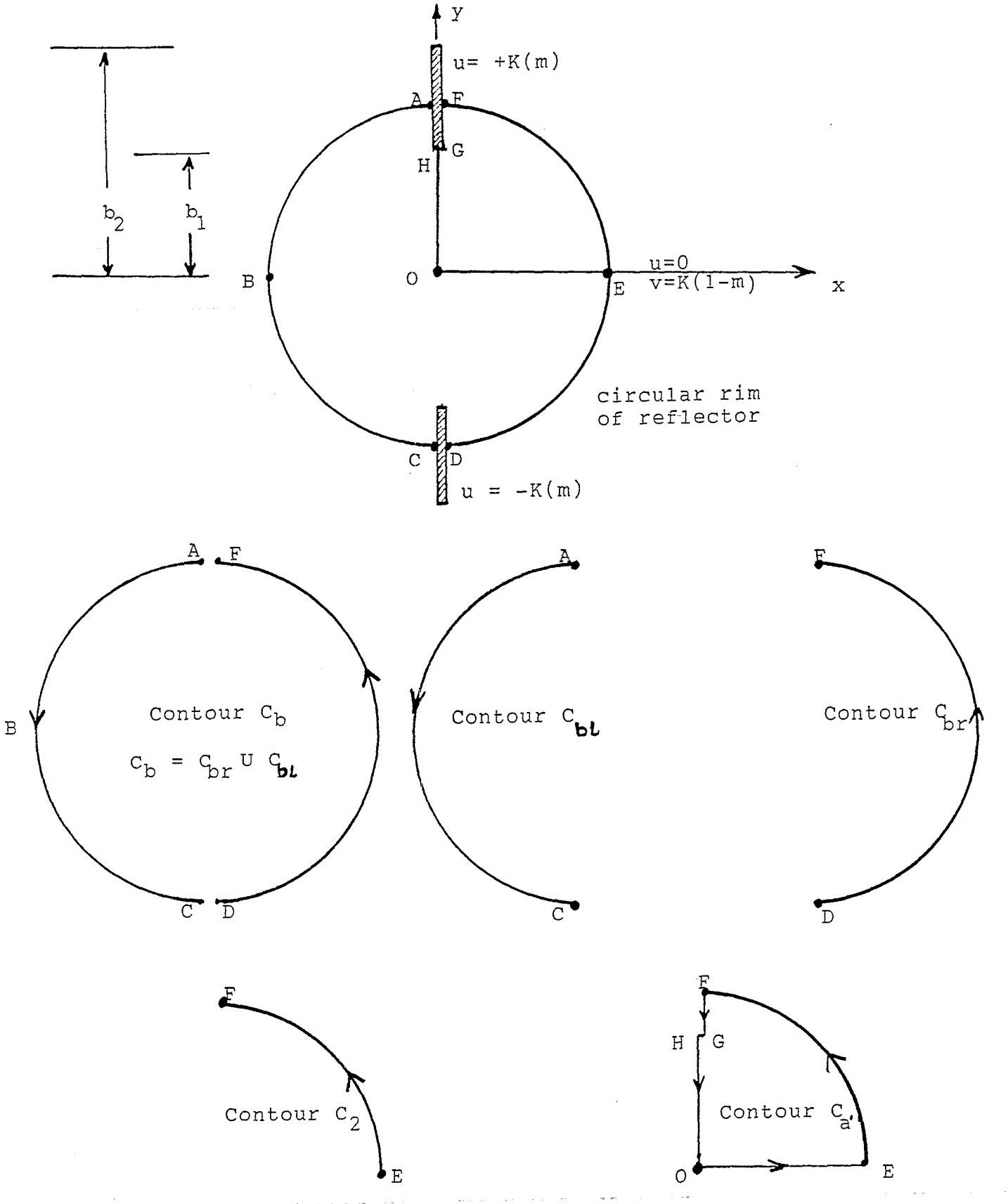

Figure 11. Geometry of the problem showing the integration paths.

The y-component of ξ reduces to

$$\begin{aligned}\xi &= -\frac{2V_0}{\Delta u}\,\frac{1}{b}\int_{C_{br}} u\,dx \\ &= -\frac{4V_0}{\Delta u}\,\frac{1}{b}\int_{C_2} u\,dx = -\frac{4V_0}{\Delta u}\,\frac{1}{b}\oint_{C'_a} u\,dx\end{aligned} \tag{62}$$

But, for a symmetric aperture where C'_a is closed containing no singularities [3],

$$\oint_{C'_a} u\,dx = \oint_{C'_a} v\,dy \tag{63}$$

or

$$\begin{aligned}\xi_y &= -\frac{4V_0}{\Delta u}\,\frac{1}{b}\oint_{C'_a} v\,dy = -\frac{4V_0}{f_g}\,\frac{1}{b}\,\frac{1}{\Delta v}\oint_{C'_a} v\,dy \\ &= -\frac{V_0}{f_g}\frac{1}{b}\,h_{a_y} \quad \text{with}\left[h_{ay} = -\frac{4}{\Delta v}\oint_{C'_a} v\,dy\right]\end{aligned} \tag{64}$$

The above integral is performed in [11] and is given by

$$h_{a_y} = \frac{\pi}{2}\,\frac{m^{-1/4}}{K(m_1)}\,b\left[1 - \frac{2}{\pi}\arcsin\left(\frac{\left[1-\sqrt{m}\right]^2}{m_1}\right)\right] \tag{65}$$

where

$$\begin{aligned} m &= (b_1/b_2)^2, \quad m_1 = (1-m) \\ f_g &= \frac{K(m)}{K(m_1)}\end{aligned} \tag{66}$$

Using (51) and (50) in (49), we get

$$\xi_y = -V_0\,\frac{\pi}{2}\,\frac{m^{-1/4}}{K(m)}\left[1 - \frac{2}{\pi}\arcsin\left(\frac{1-\sqrt{m}}{1+\sqrt{m}}\right)\right] \tag{67}$$

which is the desired result.

Asymptotic forms of h_{a_y} and ξ_y for narrow and wide plates may be derived as follows.

a) *narrow plates* [11] (plate width << plate separation)

$$\left.\begin{aligned}\left(\frac{b_1}{b_2}\right) \to 1 \quad &; \quad m \to 1 \\ m_1 \to 0 \quad &; \quad f_g \to \infty\end{aligned}\right\} \tag{68}$$

$$h_{a_y} = \underset{\substack{m \to 1 \\ m_1 \to 0}}{\text{Lim}} \left[\frac{\pi}{2} \frac{m^{-1/4}}{K(m_1)} b \left\{ 1 - \frac{2}{\pi} \arcsin\left(\frac{1-\sqrt{m}}{1+\sqrt{m}} \right) \right\} \right]$$
$$= b\left(1 - \frac{m_1}{2\pi}\right) \simeq \frac{D}{2} \tag{69}$$

Consequently,

$$\xi_y = -\frac{V_0}{f_g} \frac{1}{b} h_{a_y} \simeq -\frac{V_0}{f_g} \tag{70}$$

b) *wide plates* (plate width >> plate separation)

$$\left.\begin{aligned} \left(\frac{b_2}{b} = \frac{b}{b_1}\right) \to \infty \quad ; \quad m \to 0 \\ m_1 \to 1 \quad ; \quad f_g \to 0 \end{aligned}\right\} \tag{71}$$

We can expand $K(m)$ and the arcsin( ) in (67) as follows,

$$K(m) = \frac{\pi}{2}\left[1 + \frac{m}{4} + 0(m^2)\right] \qquad (\text{for } m \to 0) \tag{72}$$

Using

$$\arcsin(1-x) = \frac{\pi}{2} - \sqrt{2x}\left[1 + \frac{x}{12} + 0(x)\right] \qquad (\text{for } x \to 0) \tag{73}$$

we have

$$\arcsin\left(\frac{1-\sqrt{m}}{1+\sqrt{m}}\right) = \arcsin\left(1 - \frac{2\sqrt{m}}{1+\sqrt{m}}\right)$$
$$= \frac{\pi}{2} - 2\,m^{1/4}\left[1 + 0(\sqrt{m})\right] \qquad (\text{for } m \to 0) \tag{74}$$

Using (72) and (74) in (67), we get

$$\xi_y = -V_0 \frac{\pi}{2} \frac{m^{-1/4}}{\frac{\pi}{2}[1+0(m)]} \left[1 - \frac{2}{\pi}\left(\frac{\pi}{2} - 2m^{1/4}\left\{1 + 0\left(\sqrt{m}\right)\right\}\right)\right]$$
$$= -\frac{4V_0}{\pi}\left[1 + 0\left(\sqrt{m}\right)\right] \qquad (\text{for } m \to 0) \tag{75}$$

Consequently,

$$h_{a_y} = -\frac{b}{V_0} f_g\, \xi_y = \left(\frac{4b}{\pi} f_g + \cdots\right)$$
$$= \left(\frac{2D}{\pi} f_g + \cdots \cdots\right) \tag{76}$$

For wide coplanar plates considered above, one can also derive the asymptotic forms of ξ_y and h_{a_y} from the known electric field. One observes that for wide coplanar plates, the potential Φ is only a function of azimuthal angle ϕ given by

$$\Phi(\phi) = \frac{V_0}{2} \frac{\phi}{(\pi/2)} = \frac{V_0\,\phi}{\pi} \qquad \text{for} \quad -\pi/2 < \phi < \pi/2 \tag{77}$$

The electric field in the right half plane $(-\pi/2 < \phi < \pi/2)$ is given by

$$\vec{E} = -\frac{1}{\Psi} \frac{\partial \Phi}{\partial \phi} \vec{1}_\phi = -\frac{V_0}{\pi} \frac{1}{\Psi} \vec{1}_\phi \tag{78}$$

then

$$\begin{aligned} \vec{\xi} &= \int_{C_b} \vec{E}\, d\ell = 2 \int_{-\pi/2}^{\pi/2} \vec{E}\, b d\phi \\ &= -\frac{2V_0}{\pi} \int_{-\pi/2}^{\pi/2} \vec{1}_\phi\, d\phi = -\frac{2V_0}{\pi} \int_{-\pi/2}^{\pi/2} \vec{1}_y\, \cos(\phi)\, d\phi \\ &= -\frac{2V_0}{\pi} \vec{1}_y\, \sin(\phi)\Big|_{-\pi/2}^{\pi/2} = -\frac{4V_0}{\pi} \vec{1}_y \end{aligned} \tag{79}$$

resulting in

$$\xi_y = -\frac{4V_0}{\pi} \quad \text{and} \quad h_{a_y} = \left(\frac{4b}{\pi} f_g\right) \tag{80}$$

for the wide plates ($m \to 0$ or $f_g \to 0$). (80) is in agreement with (75) and (76).

References

1. C. E. Baum, "Radiation of Impulse-Like Transient Fields," Sensor and Simulation Note 321, 25 November 1989.
2. C. E. Baum, "Configurations of TEM Feed for an IRA," Sensor and Simulation Note 327, 27 April 1991.
3. C. E. Baum, "Aperture Efficiencies for IRAs," Sensor and Simulation Note 328, 24 June 1991.
4. E. G. Farr, "Analysis of the Impulse Radiating Antenna," Sensor and Simulation Note 329, 24 July 1991.
5. E. G. Farr and C. E. Baum, "Prepulse Associated with the TEM Feed of an Impulse Radiating Antenna," Sensor and Simulation Note 337, March 1992.
6. C. E. Baum and E. G. Farr, "Impulse Radiating Antennas," in *Ulta-Wideband, Short-Pulse Electromagnetics*, edited by H. L. Bertoni et al., pp. 139–147, Plenum Press, NY, 1993.
7. J. B. Keller and A. Blank, "Diffraction and Reflection of Pulses by Wedges and Corners," *Communications on Pure and Applied Mathematics*, Vol. 4, 1951, pp. 75–94.
8. P. R. Barnes, "The Axial Current Induced on an Infinitely Long Perfectly Conducting, Circular Cylinder in Free Space by a Transient Electromagnetic Plane Wave," Interaction Note 64, March 1971.
9. Y. Rahmat-Samii and D. W. Duan, "Axial Field of a TEM-Fed UWB Reflector Antenna: The PO/PTD Construction," Sensor and Simulation Note 363, 22 November 1993.
10. D. V. Giri and S. Y. Chu, "On the Low-Frequency Electric Dipole Moment of Impulse Radiating Antennas (IRAs)," Sensor and Simulation Note 346, 5 October 1992.
11. E. G. Farr, "Optimizing the Feed Impedance of Impulse Radiating Antennas Part I: Reflector IRAs," Sensor and Simulation Note 354, January 1993.
12. E. G. Farr and C. E. Baum, "Radiation from Self-Reciprocal Apertures," Sensor and Simulation Note 357, April 1993.
13. C. E. Baum, "Some Limiting Low-Frequency Characteristics of a Pulse-

Radiating Antenna," Sensor and Simulation Note 65, 28 October 1968.

14. C. E. Baum, "Some Characteristics of Electric and Magnetic Dipole Antennas for Radiating Transient Pulses," Sensor and Simulation Note 125, 23 January 1971.
15. *Electromagnetic and Acoustic Scattering by Simple Shapes,* edited by J. J. Bowman, T. B. A. Senior, and P. L. E. Uslengi, published by Hemisphere Publishing Corporation, NY (Taylor and Francis, Washington, D.C.), 1987.
16. J. Van Bladel, *Electromagnetic Fields*, Hemisphere Publishing Corporation (Revised Printing), Washington, DC, 1985.